Title

Miniature, Lightweight, High-Force, Capstan Winch for Mobile Robots

Journal

IEEE Robotics and Automation Letters, 7(4)

ISSN

2377-3766

Authors

Heap, William E
Keeley, Chris T
Yao, Elvy B
et al.

Publication Date

2022

DOI

10.1109/lra.2022.3192758

Miniature, Lightweight, High-Force, Capstan Winch for Mobile Robots

William E. Heap[1*], Chris T. Keeley[1], Elvy B. Yao[1], Nicholas D. Naclerio[2†], and Elliot W. Hawkes[2†]

***Abstract*—Actuators that apply tension forces are widely applicable in robotics. In many applications of tensile actuators, a large stroke length, high force, and small, lightweight device are important. For these requirements, the best current solution is a winch, which uses a rotating shaft to pull lightweight string. However, most winches accumulate string in a spool on their shaft which limits maximum stroke length and force at a miniature scale. An alternative is a capstan winch, in which the string wraps around the shaft in a single-layered spiral before passing off the shaft. Although high-force and high-stroke versions exist, miniaturization has not been successfully demonstrated. We present the design, modeling, and characterization of a miniaturized capstan winch. The 16 g winch is capable of lifting 4.5 kg (280x body weight) a distance of 4.3 m (67x body length) or more. We also demonstrate it actuating a jumping robot and pulling a remote-controlled car out of a ditch. Through its miniature design and high-force, high-stroke performance, our winch expands the potential capabilities of small-scale robots.**

***Index Terms*—Tendon/Wire Mechanism, Mechanism Design, Actuation and Joint Mechanisms**

I. Introduction

SMALL, mobile robots are useful for a range of fields including space exploration [1], reconnaissance [2], and search and rescue [3]. Advancements in robotics have been enabled in part by improvements in actuator technology. One class of actuation is characterized by the production of tensile forces, such as in manipulator arms [4], reconfigurable devices [5], tensegrity structures [6], exoskeletons [7], swinging robots [8], jumping robots [9]–[11] and wheeled, winching devices [12] (Fig. 1B-C).

In many applications, it is important for tensile actuators to apply a large force over a large stroke while remaining small and lightweight. However, for most tensile actuators, increasing stroke length results in a significant increase in mass, reducing the specific force of the actuator (Fig. 2). Further, many actuators [13]–[16] have a relatively low linear strain, meaning long stroke and small size are mutually exclusive.

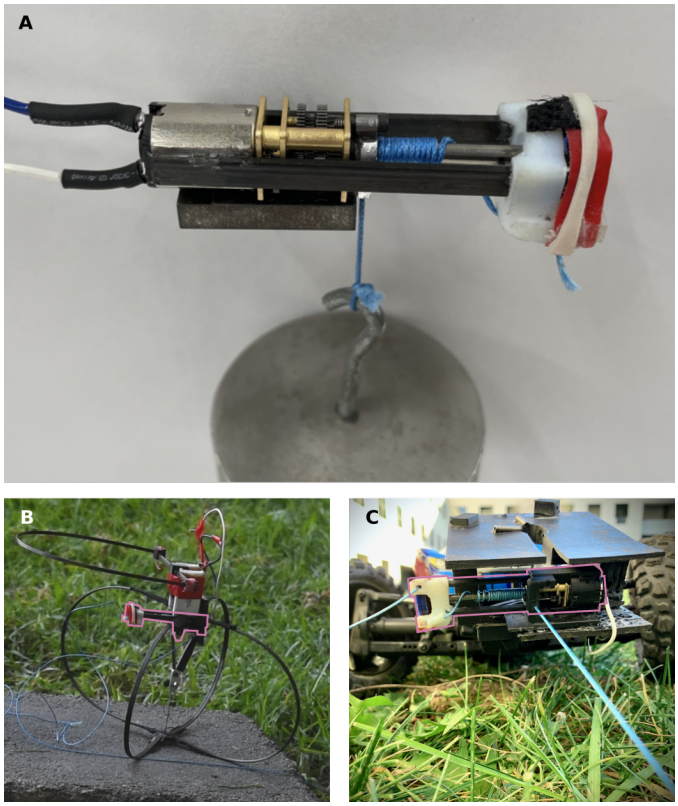

Fig. 1. A) The 16 g miniature capstan winch is shown lifting a 1 kg mass and is capable of lifting 4.5 kg, or over 280x its body weight. B) The winch winding up a spring loaded jumping robot. C) The winch pulling a remote controlled car out of a ditch. See accompanying video.

An actuator for high stroke lengths is a drum winch, which transmits tension through a flexible string wound around a cylinder attached to a drive shaft [17] (Fig. 2 illustration). However, the drum winch has three limitations that cause its specific force to decrease with stroke length. First, as stroke length increases, the size and weight of the drum must increase to accommodate more string. Second, motor torque and mass must increase with stroke length to maintain a constant output tension because as string spools around the drum, the effective drive shaft radius increases. Finally, while ultra-high-molecular-weight polyethylene (UHMWPE) fiber has very high specific tensile strength and flexibility, at small scales and high tension, we found that it tends to cut the string wrapped beneath it. This forces drum winches to use heavier oversized or cut-resistant string.

These limitations of drum winches are overcome by using a capstan winch [17, Sec. 3.3] (Fig. 2 illustration). In this type

Manuscript received: February 24, 2022; Revised May 28, 2022; Accepted June 27, 2022.

This paper was recommended for publication by Editor Clement Gosselin upon evaluation of the Associate Editor and Reviewers' comments. This work was supported by an Early Career Faculty grant from NASA's Space Technology Research Grants Program, the NSF (grant #1944816), and a UC Santa Barbara Undergraduate Research and Creative Activities grant. The work of N.N. was supported by a NASA Space Technology Research Fellowship.

[1]College of Engineering, University of California, Santa Barbara, CA 93106 USA

[2]Department of Mechanical Engineering, University of California, Santa Barbara, CA 93106 USA

*Corresponding author. Email: wheap@ucsb.edu

†Co-last author

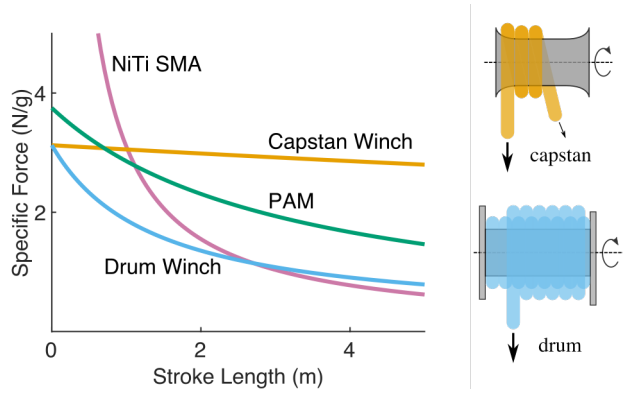

Fig. 2. The specific force of the capstan winch scales better than other linear actuators and has the highest specific force at high stroke lengths. Values are plotted for NiTi shape memory alloy (SMA) [16], the presented capstan winch, a drum winch, and a pneumatic artificial muscle [14] with a 32 g air compressor (2x the capstan winch mass). Values for the capstan winch are experimental. Values for the drum winch are identical to the capstan winch, but with the assumption that drum size and therefore motor torque and mass increase with stroke length.

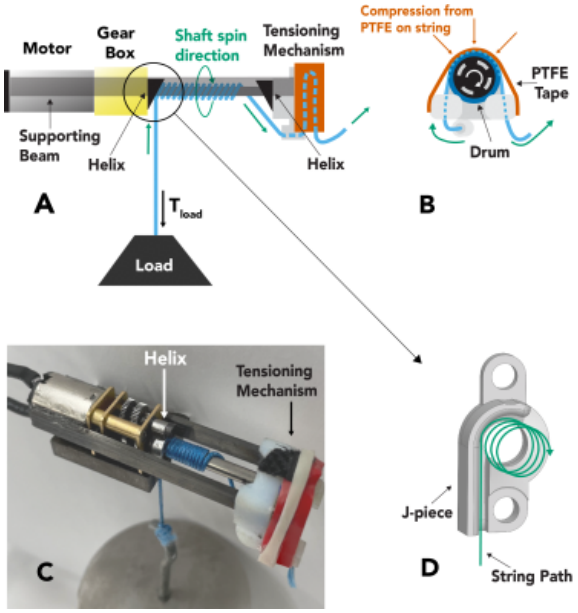

Fig. 3. A) Side view illustration of the miniature capstan winch with core components labeled. B) End view showing the tensioning mechanism. C) Isometric photo of the winch. D) CAD rendering of the helix and "J" piece.

of winch, the string is wrapped 3-5 times around the shaft, or capstan, in a single-layered spiral with the string's free end passed on to an external tensioner. Since friction increases exponentially as the string wraps around the shaft (see (1)), a low string tension on the free end can support a very high tension on the load side. As the shaft rotates, the string slides along the tapered shaft to make room for new string, increasing its frictional losses compared to a drum winch, but enabling infinite stroke at a constant force and gear ratio.

Despite their high mass-efficiency at long stroke lengths, capstan winches have not been implemented in small, lightweight robots because of challenges inherent in miniaturization. Most current capstan winches are designed for marine or industrial applications and use heavy steel cables and rope with a human operator to tension the free end of the cable. Instead of a human tensioner, sail boats often use "self-tailing" capstan winches with serrated teeth [18] to tension the free end (or "tail") of the cable or rope. This design cannot be miniaturized to work with lightweight string because the self-tailing teeth would damage the string. Further, the taper of a capstan winch (Fig. 2 illustration) used to slide string along the shaft is difficult to miniaturize without compromising shaft strength.

To address these limitations, we present a miniature capstan winch for mobile robots (Fig. 1A). It features 10-20 wraps around the shaft, rather than the typical 3-5, that allow it to use low-friction, high-specific-strength UHMWPE string, an integrated self-tensioning mechanism for self-tailing, and a helical plate to avoid using a tapered shaft. The miniature capstan winch is a mass-efficient, small-scale actuator capable of applying high tensile forces over large stroke lengths.

In this paper we present the design and modeling of the winch, as well as experimental characterization of performance and power losses. We also demonstrate its applicability in actuating small-scale mobile robots: it compresses a spring-actuated jumping robot, hoists a 4.5 kg load a distance of 4.3 m, and tows a remote-controlled vehicle out of a ditch.

II. Design

The core components of the presented winch are the motor, shaft, string, helix plate, and tensioning mechanism shown in Fig. 3. The motor is attached directly to one end of the shaft and provides power to the winch. The string is wrapped many times around the shaft with one end attached to a load while the other passes through the tensioning mechanism.

The helix plate is mounted to the motor gearbox, shown in Fig. 3D, and pushes the wraps of string along the shaft away from the motor. This makes room for new wraps as the oldest wraps are removed through the tensioning mechanism. The plate is made of 3/4 of an extruded helix with a pitch equal to 4/3 the thickness of the string. As the shaft rotates, the string is pulled along the surface of the helix plate, such that after one turn, the string is moved axially along the shaft by one string thickness. Without the helix, the string will wrap over itself and prevent the capstan winch from working.

The small "J"-shaped piece covers the helix plate to guide string around the contour of the helix and onto the shaft regardless of tension. Without it, the string does not wind properly without high tension. A second helix and "J" covering is added at the opposite end of the shaft to enable smooth operation of the winch in both directions. This helix pushes the wraps toward the motor as string is brought onto the shaft through the tensioning mechanism and the load is lowered.

The frictional tensioning mechanism ("tensioner") on the non-load side (free end) of the string provides a small holding tension that allows the capstan winch to operate without an external holding force. The tensioner consists of a high friction drum fixed to the motor shaft that slides against a low friction film attached to the motor by support beams (Fig. 3 B). The diameter and therefore tangential velocity of the tensioner drum is higher than that of the motor shaft. As the

string passes through the tensioner, friction from the relative movement between the string and the drum tensions the string. The capstan winch can also operate in reverse, but since the tensioner is only on one end of the winch, a load must be provided to reverse operation.

III. Modeling

A. Capstan Winch Maximum Tension Model

In this section, we model the maximum tension the capstan winch can apply as a function of holding tension and wrap angle. The general model relating maximum load tension T_{load} and holding tension T_{hold} (where $T_{load} > T_{hold}$) around a capstan (as drawn in Fig. 4) is

$$T_{load} = T_{hold} e^{\mu \theta_{total}} \tag{1}$$

where μ is the coefficient of friction between the string and capstan, and θ_{total} is the total angle swept by the string as it wraps around the shaft [19]. Note that this equation assumes static equilibrium, and acceleration between the capstan and the string will only occur if $T_{load} > T_{hold} e^{\mu \theta_{total}}$.

1) Incorporating Power Law Friction Model: Equation (1) can be used with either Amonton's law friction, or power law friction. Amonton's first law of friction is simply

$$F_f = \mu N \tag{2}$$

where F_f is friction force, N is normal force, and μ is a constant static or dynamic friction coefficient [20]. However, the linear relationship in (2) is meant for solid materials, and is less accurate for viscoelastic materials including polymer string [21]. Instead, a power law can be used:

$$F_f = \alpha N^n \tag{3}$$

where α and n are constants specific to the string and shaft material [22], [23].

As shown in [23, eq. (19), (20)], (1) can be written using power law friction by replacing μ with an effective μ_e of:

$$\mu_e = \alpha \left(\frac{R}{T_{load}} \right)^{1-n} \frac{ln(1+K)}{K} \tag{4}$$

where

$$K = -\alpha(1-n) \left(\frac{R}{T_{load}} \right)^{1-n} \theta_{total}$$

and R is capstan radius as shown in Fig. 4. Notably, μ_e is dependent on T_{load} and θ_{total}, which better matches experimental data compared to Amonton's law (see Section V-B).

2) Limitations: While this model is useful for finding feasible T_{load}, T_{hold}, and θ_{total} combinations, it is limited by the assumption of a static equilibrium case where the frictional force is assumed to be at its limit along the entire length of wrapped string. Therefore, for cases where T_{load} is not at its limit and slipping between the string and shaft is not accelerating (or "catastrophic"), this model does not provide a description of state of the string along its wraps. Despite this limitation, the combination of (1) and (4) provide a useful way to model the maximum operating parameters of a capstan winch with viscoelastic materials.

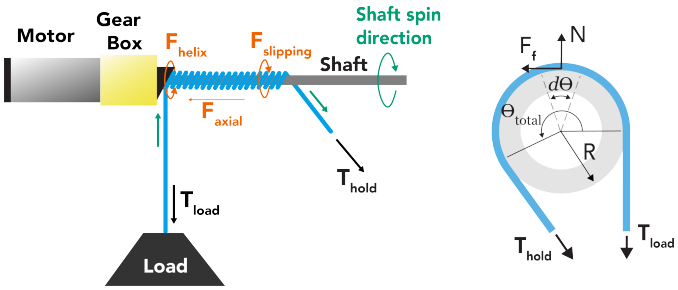

Fig. 4. Left: Internal forces in the capstan winch used in (6)-(11). Frictional force F_{axial} acts against the string along the axis of the shaft, F_{helix} along the helix, and $F_{slipping}$ tangentially to the shaft as drawn. Right: The geometry of a capstan winch showing relevant variables used in (1), (2), (3), and (4).

B. Efficiency

This section characterizes the efficiency (ratio of output power to input power) of the miniature capstan winch, an important metric of actuators for mobile robot applications: higher efficiency means reduced mass and required power output of the robot's energy source. Such characterization offers insight as to how design parameters should be tuned to improve efficiency for a given application. We note that for efficiency characterization, we are interested in the standard use case when the load is not at its maximum and the string is not about to catastrophically slip, meaning the above model is not applicable (though very slow, steady-state slipping may occur during the standard use case, as seen in Section V-D). Accordingly, we derive new relations that allow us to determine the necessary values to estimate efficiency during standard use.

The input power $P_{gearbox}$ is the power input from the motor after the gearbox, and the output power P_{out} can be determined as the input power minus three primary power losses, which are all friction based and not found in drum winches. The first, P_{axial}, is from the string sliding along the axle. The second, P_{helix}, is from the string sliding against the helix plate. The third, P_{slip}, is from very slow, steady rotational slipping between the string and the axle. In summary:

$$P_{out} = P_{gearbox} - P_{axial} - P_{helix} - P_{slip}. \tag{5}$$

All of the power loss terms are dependent on internal frictional forces described below and in Fig. 4; knowing these forces is necessary to determine the power losses (described in the following subsections), and thus efficiency. The first force is F_{axial}, a frictional force which resists the axial sliding of the string along the shaft. The second force is $F_{slipping}$, a frictional force which resists the rotation of the string relative to the shaft. As the magnitude of both F_{axial} and $F_{slipping}$ are determined by an identical string-shaft interface with the same normal force distribution and material properties, we assume $F_{axial} \approx F_{slipping}$. This is similar to how a car tire will have the same frictional force in the fore-aft direction as the sideways direction.

The third force is F_{helix}, a frictional force which resists the rotation of the string relative to the surface of the helix plate. As this force involves the viscoelastic polymer string sliding against aluminum, we use the power law to describe

the frictional force generated. We also note that the effective normal force pressing the string into the helix must also equal F_{axial} and therefore:

$$F_{helix} = \alpha_h N^{n_h} = \alpha_h F_{axial}^{n_h} \tag{6}$$

where the constants α_h and n_h are specific to the string-helix interaction and are reported in Section V-E4.

1) Axial Power Loss: P_{axial} is caused by the string sliding axially along the shaft and is the product of force and linear velocity:

$$P_{axial} = F_{axial} \frac{b}{2\pi} \dot{\theta} \tag{7}$$

where b is the distance the string travels along the shaft every revolution, and $\dot{\theta}$ is the angular velocity of the string (which may be slightly different from the angular velocity of the shaft due to slow, steady slipping). F_{axial} is measurable while b is a known quantity determined by the helix pitch. $\dot{\theta}$ is derived from measured linear lift speed as:

$$\dot{\theta} = \frac{\dot{y}}{R + \frac{d_{string}}{2}} \tag{8}$$

where $\dot{y}$ is lifting speed of the load, R is the radius of the capstan winch shaft, and d_{string} is the diameter of the string.

2) Helix Power Loss: P_{helix} is caused by the string rotating against the helix plate. This friction generates a torque $\tau_{friction}$, and thus P_{helix} can be written as torque times angular velocity:

$$P_{helix} = \tau_{friction} \dot{\theta}. \tag{9}$$

$\tau_{friction}$ is difficult to measure, but can be written in terms of F_{helix} by integrating the frictional moment over the area of a disk rotating against a plate with a uniform normal force and coefficient of friction (see [24] for derivation). Thus,

$$\tau_{friction} = \frac{2}{3} F_{helix} \left(\frac{(R + d_{string})^3 - (R)^3}{(R + d_{string})^2 - (R)^2} \right) \tag{10}$$

where F_{helix} can be found in terms of F_{axial} with (6).

3) Slipping Power Loss: P_{slip} is caused by slow, steady relative rotational movement between the string and the shaft. The tensioned string constantly applies a compressive force onto the shaft which generates a frictional force opposing relative motion between the string and the shaft. P_{slip} is written as a deconstructed torque times an angular velocity:

$$P_{slip} = F_{slipping} R (\dot{\theta}_{shaft} - \dot{\theta}) \tag{11}$$

where $\dot{\theta}_{shaft} - \dot{\theta}$ is the difference in rotational velocity between the shaft and string.

IV. Prototype Fabrication

This section describes the fabrication of the miniature capstan winch prototype as described in Section II. The winch has a mass of 16 g and overall dimensions of 64.5 mm by 19 mm by 21.5 mm. The winch mechanism is only 6 g, while the remaining 10 g is a brushed DC motor with a 1000:1 gearbox (Pololu Item number 1595). The 3mm D-profile motor shaft was turned down to a 2mm diameter, and a 30 mm long 3 mm OD 2 mm ID steel shaft was adhered to it with epoxy (JB Cold Weld). The body of the tensioning mechanism was 3-d printed in a stiff resin (Objet30 RGD450) and mounted to the motor body by two rectangular carbon fiber beams with cyanoacrylate adhesive (Loctite 401). The tensioning drum is 12.5 mm in diameter at the center and 13 mm at the edges with a 0.6 mm thick high-friction rubber coating (Dycem). Wrapped around the drum is a PTFE film adhered with electrical tape and cryanoacrylate to the ends of the carbon fiber support beams. The helices were machined from 6061 aluminum and are mounted to the gearbox housing and tensioning mount with screws. The winching string is 0.7 mm thick 150-lb-test braided UHMWPE (Piscifun Onyx). UHWWPE fiber was chosen for its high specific tensile strength and flexibility. This thickness was chosen for greater abrasion resistance and high factor of safety.

V. Experimental Characterization

This section describes experimental methods and results that first validate our capstan winch maximum tension model and second characterize the internal forces, power losses, and efficiency of the capstan winch.

A. Experimental Setup

The test setup shown in Fig. 5 was used to characterize the capstan winch under different string tensions and numbers of wraps. It recorded axial force, motor current and voltage, shaft speed, and weight lifting speed. The capstan winch was mounted in a 3D-printed frame and attached to a Mark-10 M3-100 force sensor to measure axial force, and to a magnetic encoder to measure shaft rotation speed. The string was loaded on one end with a hanging load mass (T_{load}) attached to a belt and rotary encoder system to measure its lifting speed, and on the other end to a lighter mass that provided the holding tension (T_{hold}).

The winch axial force, slipping, and power loss tests were performed without the tensioning mechanism in order to easily vary the T_{hold} applied. As a result, the net load lifted by the winch was equal to $T_{load} - T_{hold}$ where T_{load} was kept at a constant 27 N and T_{hold} was varied from 0.25 N to 5.89 N. When testing the integrated system the tensioning mechanism was included and thus net load lifted by the winch was equal to T_{load}. T_{load} was varied from 16.3 N to 60.8 N while the T_{hold} provided by the tensioning mechanism was constant at 4.5 N.

In all trials the winch was run at a constant voltage for 5 seconds to reach a steady state before collecting data for 10 seconds. Each test was run three times and the standard deviation calculated using the data collected every 20 ms for axial force and current, while for the shaft and load speed, the average speed of each trial was used.

B. Maximum Tension Model Validation

To validate the maximum tension model presented in (1) and (4) for our system, we measured the T_{load} required to accelerate a constant T_{hold} for a given θ_{total} at various shaft rotation speeds. Results are shown in Fig. 6, along with a power law curve fit ($\alpha = 0.040$ and $n = 0.506$) to the

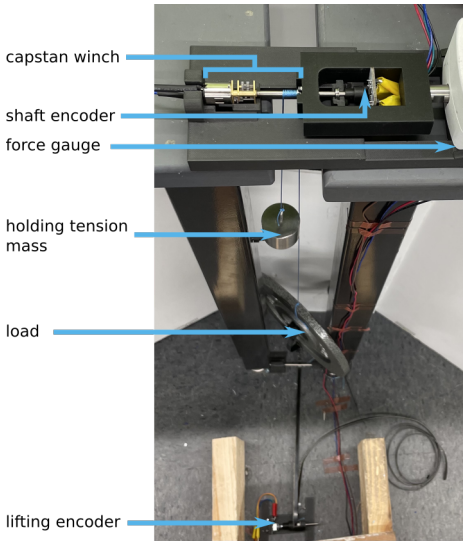

Fig. 5. Setup used to characterize the capstan winch. As the winch lifts a load, the string is pressed against the helix plate which is attached to the force gauge to measure F_{axial}. A mass was used for holding tension in this experimental characterization instead of the tensioning mechanism. The shaft encoder measures shaft speed while the lifting encoder measures the speed of the load.

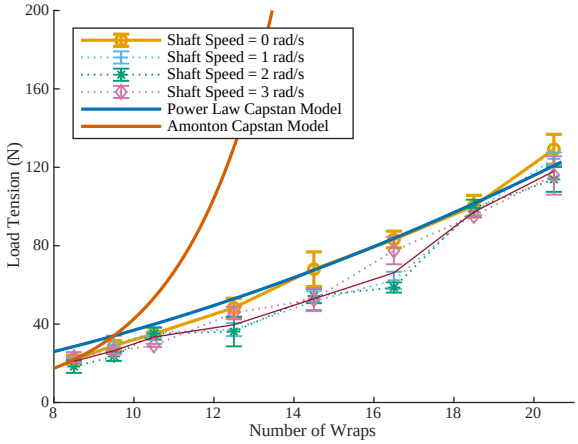

Fig. 6. Maximum load tension (T_{load}) as a function of wraps around the shaft for a constant holding tension of 0.5 N. T_{load} is far lower than would be expected by (1) and Amonton's law (2). It is better modeled by a fitted power law friction (3)(4).

data with no shaft rotation, and a curve using Amonton's law with μ derived from the smallest wrap angle data. The Amonton capstan model over-predicts the behavior of the system while the power law provides a better model and is useful for predicting the limits of the capstan winch's operating parameters. In addition, shaft speed does not appear to strongly affect the results.

C. Axial Force Results

Axial force is required to determine power losses and thus efficiency in the next section. It was measured as a function of string wraps and holding tension and is plotted in Fig. 7. The results show that axial force increases with both the number of string wraps and holding tension. Although the maximum tension model does not exactly model this case since the string

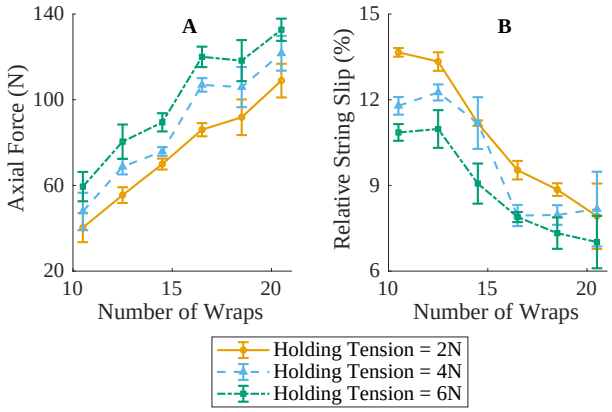

Fig. 7. A) Axial force (F_{axial}) as a function of the number of wraps of string. B) Steady slipping speed between the string and shaft relative to shaft speed as a function of the number of wraps of string. For both plots, three holding tensions were tested while load tension was constant at 27 N.

is not about to catastrophically slip, it does predict these trends. Both number of string wraps and holding tension correspond to an increase in μ_e in (4) and an increase in the total tension in (1); this increases total normal force and thus frictional force F_{axial}.

D. String Slip Results

We found that the string slips relative to shaft rotation at a slow, steady rate in all tested conditions, as shown in 7. However, this steady slip occurs without any transition to accelerating (catastrophic) slipping. This steady slipping is likely caused by the slow, steady axial slipping of the string along the shaft. Slip decreases with the number of string wraps and with increased holding tension, which is expected as both factors increase friction (see (4) and (1)).

E. Power Loss Results

Power from the motor was input to the capstan winch and output as: useful power, the three power losses described in Sec. III-B, and test setup losses. Results as a function of wrap angle and holding tension are plotted in Fig. 8. Fig. 9 shows a more detailed plot of power and efficiency as a function of holding tension for 18.5 wraps. This number was chosen to give enough friction to test low holding tensions, but not enough to overload the motor under repeated testing. In both plots the height of the stacked bars represent our estimation for the power output and losses of the winch. On average these bars account for 90% of input power. This indicates our modeling of power losses in Section III-B captures most sources of loss. A possible unaccounted loss is the friction between the string and "J" piece. Details on the power input and outputs are given below.

1) Shaft Input power: This was found by relating measured motor current to the motor manufacturer's output power characterization curve (measured at the output of the gearbox). As the number of wraps and T_{hold} increase, the load on the motor increases, causing it to deliver more power.

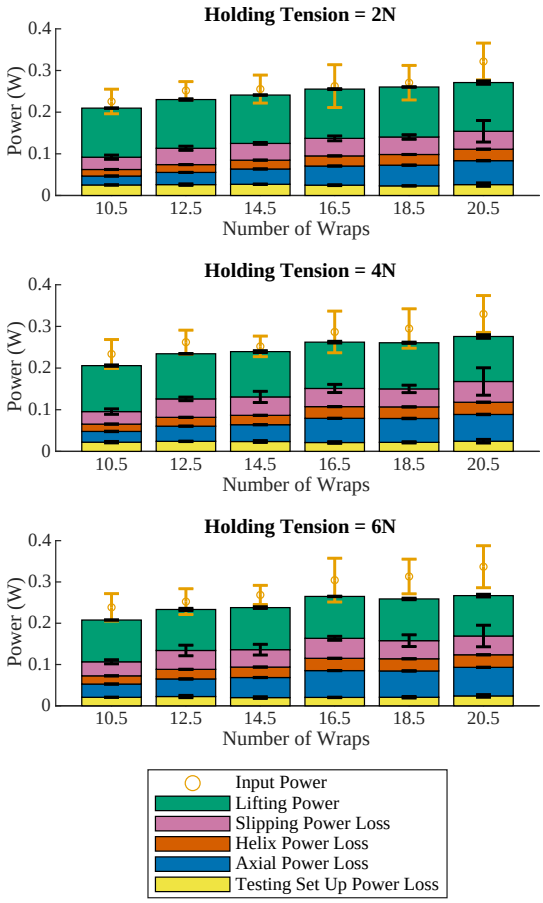

Fig. 8. Power characterization stacked bar plots displaying power input, output, and losses as a function of the number of string wraps. Separate plots for three different holding tensions at a constant load tension of 27 N.

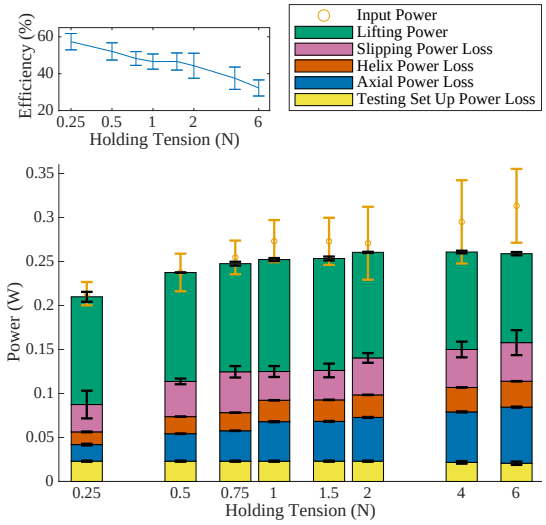

Fig. 9. Power characterization stacked bar plots displaying power outputs and losses as a function of holding tension. Inset plot shows winch efficiency (input power divided by lifting power) as a function of holding tension. Note that x-axis of both plots are log scales. 18.5 wraps were used with a constant loading tension of 27 N. At less than 0.25 N of holding tension, the capstan winch does not have enough friction to support the load.

2) Lifting power: The useful mechanical output power of the capstan winch was calculated as the net load times lifting speed. It remained relatively constant with number of wraps and holding tension, so overall efficiency decreased as holding tension and power losses increased (Fig. 9 inset).

3) Slipping power loss: Loss from the relative rotation between the string and the shaft was calculated using (11). It is proportional to both axial force and relative steady slipping velocity, which have opposite linear relationships with number of wraps and holding tension as shown in Figure 7. Overall, slipping power loss increased slightly with wraps and holding tension.

4) Helix power loss: This was calculated using (9). The values of $\alpha = 0.41$ and $n = 0.57$ against the helix plate were found with a similar procedure as in Section V-B, but with an aluminum shaft of the same material as the helix plate with 3 rad/s of slip. Helix power loss increases with number of wraps and holding tension due to the increased axial force.

5) Axial power loss: Loss due to the string sliding axially down the shaft was calculated using (7). Axial force and therefore power loss increased with holding tension and number of wraps, as expected by the increase in N_{total} and therefore friction.

6) Testing set up power loss: Testing setup losses were accounted for by running the winch without letting the string touch the helix, which eliminated string slip, slipping losses, helix losses, and axial losses. This test was performed for every T_{load}, T_{hold}, and θ_{total} combination used in testing. These losses remained constant across testing conditions, and are likely due to friction between the shaft, bearings, and helix.

F. Integrated Device Performance

We measured the performance of the capstan winch with the tensioning mechanism using the setup described in Sec. V-A, but without the mass that provided holding tension. The tensioning mechanism adds an additional power loss to provide T_{hold}. The lifting power of the winch was measured as a function of load from 16.3 N to 60.8 N and is plotted along with calculated total efficiency (with electrical power as the input) and efficiency excluding the motor (with motor shaft power as the input) in Fig. 10. The output power and efficiency of the capstan winch increased with load, peaking at 36.5% at a load of 50 N.

The capstan winch can lift at least 110 N, but at higher loads its lifetime was reduced. The winch successfully hoisted a 44 N load 4.3 m in 12.5 minutes without failure (Section VI-A). However, at a load of 110 N its lifetime was reduced to less than a minute. Typical failure modes included motor failure from overheating, gearbox failure from gears shearing, and the shaft decoupling from the motor output shaft due to high axial force.

G. Performance Compared To Drum Winch

The performance of the capstan winch was compared to a drum winch with the same motor, gearbox, and shaft. The current drawn by the motor to winch 44.5 N for both winch types was measured and is plotted in Fig. 11. Note that for

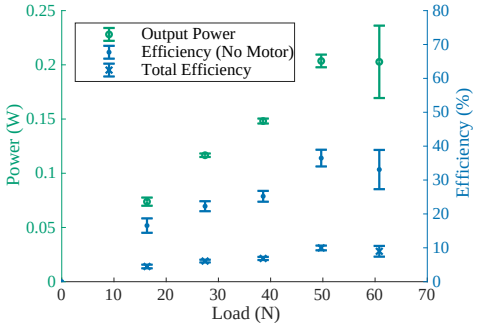

Fig. 10. Power and efficiency plotted as a function of net load on the winch. Output power is calculated from the speed of the load times weight. "Total Efficiency" incorporates the inefficiency of the motor and gearhead while "Efficiency Excluding Motor" does not.

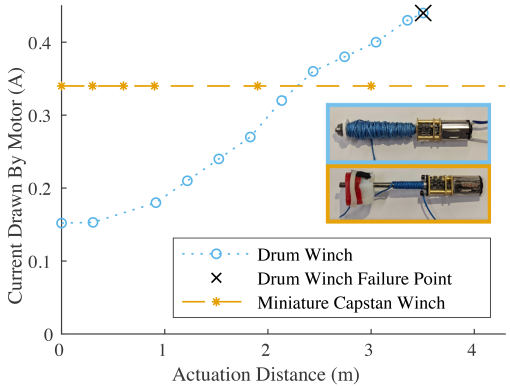

Fig. 11. Motor torque required to pull 44.5 N for both the capstan winch and a drum winch. The drum winch motor failed at 3.5 m stroke length while the torque for the capstan winch remains constant without failure. The upper inset photo shows the drum winch at failure while the lower photo shows the miniature capstan winch.

these motors, current draw is proportional to motor torque output. While the drum winch is very efficient (1% loss at 0 m of actuation), as it spooled string its effective radius increased from 3 mm to 7 mm, increasing torque until the motor failed after pulling 3.5 m. In contrast, the capstan winch runs at a constant torque regardless of actuation distance. Due to its inefficiencies it requires more torque than the drum winch at low actuation distances, but it can actuate much longer distances (limited by the length of the string).

VI. Robot Applications

To demonstrate the utility of the miniature capstan winch, it was employed in a jumping robot, a hoist, and on a remote controlled car. We used the results from our characterization tests to optimize performance by reducing tensioner mechanism T_{hold} to 2.2 N and used 16.5 wraps, which was the minimal number for the given loads and T_{hold} (and thus caused the minimal amount of loss).

A. Jumping Robot and Hoist

In the first demonstration, the winch was used to actuate a jumping robot by winching 0.5 m of string at a force increasing from 47 N to 112 N to compress the carbon fiber legs of a 64 g jumping robot as described in [11] (Fig. 12A,B). This

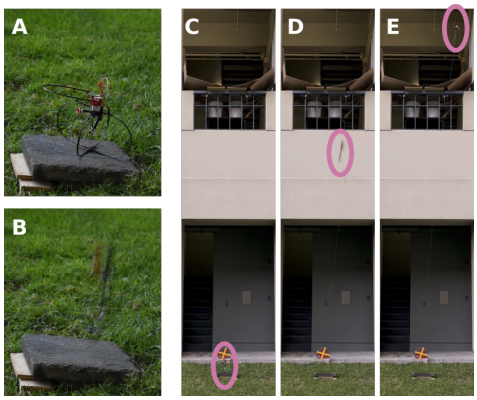

Fig. 12. The capstan winch powers a jumping robot. A) The jumping robot ready to jump after being compressed by the miniature capstan winch. B) The jumping robot rapidly decompressing and jumping. C-E) The jumping robot jumps 5 m up to a cardboard platform on a second story ledge.

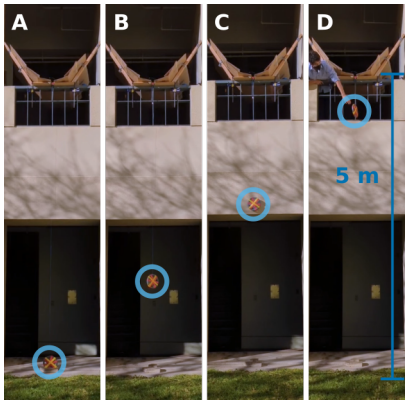

Fig. 13. After jumping to a ledge, the winch hoists a 4.5 kg mass 4.3 m up to itself.

compression length is far longer than other jumpers [9], [10]. The carbon fiber was then released and the robot jumped up 5 m onto a ledge with a custom platform (Fig.12C-E). While on the ledge, the winch hoisted a 4.5 kg mass (280 times winch mass) 4.3 m (67 x winch body length) up to the ledge in 12.5 minutes (Fig. 13).

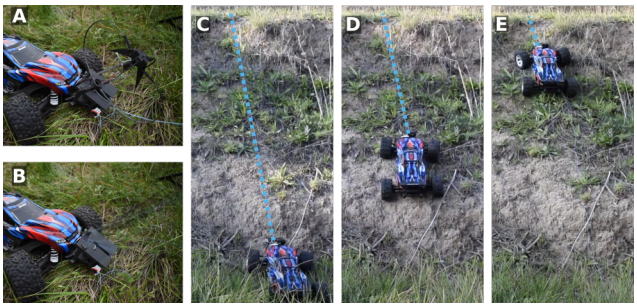

Fig. 14. The capstan winch rescues a car. A) 3 kg remote-controlled car with custom grapple launcher in a ditch. B) Grapple launched 3 m up and outside of the ditch. C-E) Car being winched 2 m up and out of the ditch, with the winch string traced by the dotted blue line.

B. Grapple Winch

In the second demonstration, the winch was used with a grapple launcher to tow a remote-controlled car out of a ditch (Fig. 14). The capstan winch was attached to a spring loaded grapple and mounted to the front of a Traxxas Rustler 4x4 remote-controlled car. After getting stuck in a ditch, the grapple was remotely launched up a height of 3 m where it locked onto a bush outside the ditch. The miniature capstan winch then pulled the 3 kg car 2 m up and out of the ditch in 28 minutes (slower than the hoisting demonstration because voltage was limited to 3.7 V due to battery constraints). With a reusable latch, the winch could reset, relaunch, and re-winch the grapple.

VII. Discussion and Conclusion

Lightweight, high-force and high-stroke actuators are useful for a variety of robotic applications. To this end, we have developed a miniature capstan winch that is more mass-efficient and miniaturaizable than drum winches and other actuators at long stroke lengths (Figures 2 and 11). We modeled and experimentally validated its performance and efficiency as a function of string wraps and tension, finding optimal parameters for sample robotic applications in jumping, hoisting, and towing (Section VI).

Although we were able to model the behavior of the friction along the length of the string-shaft interface in the maximum load case, there is no analytical model in the standard use case when not at maximum load (about to catastrophically slip). To add to the complexity, the capstan winch also has a small amount of steady-state slip during standard use. These behaviors likely require computational modeling to describe, which could provide more insight on design optimization.

The efficient mass scaling and small size of the miniature capstan winch make it useful for lightweight robot applications requiring high stroke length. Besides compressing a jumping robot or towing a rover out of a ditch, potential applications include exploring caves or assembling structures, telecommunication equipment, and solar panels on earth or in space. With these advantages and potential uses, the miniature capstan winch expands the capabilities of small, mobile robots.

References

[1] J. Balaram, M. Aung, and M. P. Golombek, "The ingenuity helicopter on the perseverance rover," *Space Science Reviews*, vol. 217, no. 4, pp. 1–11, 2021.

[2] E. Olson, J. Strom, R. Morton, A. Richardson, P. Ranganathan, R. Goeddel, M. Bulic, J. Crossman, and B. Marinier, "Progress toward multi-robot reconnaissance and the magic 2010 competition," *Journal of Field Robotics*, vol. 29, no. 5, pp. 762–792, 2012.

[3] C. D. Bellicoso, M. Bjelonic, L. Wellhausen, K. Holtmann, F. Günther, M. Tranzatto, P. Fankhauser, and M. Hutter, "Advances in real-world applications for legged robots," *Journal of Field Robotics*, vol. 35, no. 8, pp. 1311–1326, 2018.

[4] T. Lens and O. Von Stryk, "Investigation of safety in human-robot-interaction for a series elastic, tendon-driven robot arm," in *2012 IEEE/RSJ International Conference on Intelligent Robots and Systems*. IEEE, 2012, pp. 4309–4314.

[5] J. Kaufmann, P. Bhovad, and S. Li, "Harnessing the multistability of kresling origami for reconfigurable articulation in soft robotic arms," *Soft Robotics*, 2021.

[6] D. S. Shah, J. W. Booth, R. L. Baines, K. Wang, M. Vespignani, K. Bekris, and R. Kramer-Bottiglio, "Tensegrity robotics," *Soft robotics*, 2021.

[7] G. M. Bryan, P. W. Franks, S. C. Klein, R. J. Peuchen, and S. H. Collins, "A hip–knee–ankle exoskeleton emulator for studying gait assistance," *The International Journal of Robotics Research*, vol. 40, no. 4-5, pp. 722–746, 2021.

[8] D. Cunningham and H. H. Asada, "The winch-bot: A cable-suspended, under-actuated robot utilizing parametric self-excitation," in *2009 IEEE International Conference on Robotics and Automation*. IEEE, 2009, pp. 1844–1850.

[9] M. A. Woodward and M. Sitti, "Multimo-bat: A biologically inspired integrated jumping–gliding robot," *The International Journal of Robotics Research*, vol. 33, no. 12, pp. 1511–1529, 2014.

[10] V. Zaitsev, O. Gvirsman, U. B. Hanan, A. Weiss, A. Ayali, and G. Kosa, "A locust-inspired miniature jumping robot," *Bioinspiration & biomimetics*, vol. 10, no. 6, p. 066012, 2015.

[11] E. W. Hawkes, C. Xiao, R.-A. Peloquin, C. Keeley, M. R. Begley, M. T. Pope, and G. Niemeyer, "Engineered jumpers overcome biological limits via work multiplication," *Nature*, vol. 604, no. 7907, pp. 657–661, 2022.

[12] I. A. Nesnas, L. Kerber, A. Parness, R. Kornfeld, G. Sellar, P. McGarey, T. Brown, M. Paton, M. Smith, A. Johnson *et al.*, "Moon diver: a discovery mission concept for understanding the history of secondary crusts through the exploration of a lunar mare pit," in *2019 IEEE Aerospace Conference*. IEEE, 2019, pp. 1–23.

[13] K. Suzumori and A. A. Faudzi, "Trends in hydraulic actuators and components in legged and tough robots: a review," *Advanced Robotics*, vol. 32, no. 9, pp. 458–476, 2018.

[14] N. D. Naclerio and E. W. Hawkes, "Simple, low-hysteresis, foldable, fabric pneumatic artificial muscle," *IEEE Robotics and Automation Letters*, vol. 5, no. 2, pp. 3406–3413, 2020.

[15] Y. Chen, H. Zhao, J. Mao, P. Chirarattananon, E. F. Helbling, N.-s. P. Hyun, D. R. Clarke, and R. J. Wood, "Controlled flight of a microrobot powered by soft artificial muscles," *Nature*, vol. 575, no. 7782, pp. 324–329, 2019.

[16] J. M. Jani, M. Leary, A. Subic, and M. A. Gibson, "A review of shape memory alloy research, applications and opportunities," *Materials & Design (1980-2015)*, vol. 56, pp. 1078–1113, 2014.

[17] I. Samset, *Winch and cable systems*. Springer Science & Business Media, 1985, vol. 18.

[18] J. Guangorena, "Self-tailing winch," Jul. 13 1976, uS Patent 3,968,953.

[19] I. Stuart, "Capstan equation for strings with rigidity," *British Journal of Applied Physics*, vol. 12, no. 10, p. 559, 1961.

[20] M. Mate and R. Carpick, *Tribology on the Small Scale: A Modern Textbook on Friction, Lubrication, and Wear*. Oxford Scholarship Online, 2019, vol. 2.

[21] S. Ramkumar, R. Rajanala, S. Parameswaran, R. Paige, A. Shaw, D. Shelly, T. Anderson, G. Cobb, R. Mahmud, C. Roedel *et al.*, "Experimental verification of failure of amontons' law in polymeric textiles," *Journal of applied polymer science*, vol. 91, no. 6, pp. 3879–3885, 2004.

[22] H. Howell, "24—the general case of friction of a string round a cylinder," *Journal of the Textile Institute Transactions*, vol. 44, no. 8-9, pp. T359–T362, 1953.

[23] X. Gao, L. Wang, and X. Hao, "An improved capstan equation including power-law friction and bending rigidity for high performance yarn," *Mechanism and Machine Theory*, vol. 90, pp. 84–94, 2015.

[24] "Disk friction," in *Mechanics Map Open Textbook Project*, J. Moore, M. Chatsaz, A. d'Entremont, J. Kowalski, and D. Miller, Eds., accessed: 23 February 2022.